

1 **The impacts of changing transport and precipitation on pollutant**
2 **distributions in a future climate**

3 Yuanyuan Fang^{1,2}, Arlene Fiore², Larry Horowitz^{1,2}, Anand Gnanadesikan^{1,2}, Isaac Held^{1,2},
4 Gang Chen³, Gabriel Vecchi², Hiram Levy²

- 5 1. Atmospheric and Oceanic Sciences Program, Princeton University, Princeton, NJ, 08540
6 2. Geophysical Fluid Dynamics Laboratory, National Oceanic and Atmospheric
7 Administration, Princeton, NJ, 08540
8 3. Dept of Earth and Atmospheric Sciences, Cornell University, Ithaca, NY, 14853

9

10

Abstract

11 Air pollution (ozone and particulate matter in surface air) is strongly linked to
12 synoptic weather and thus is likely sensitive to climate change. In order to isolate the
13 responses of air pollutant transport and wet removal to a warming climate, we examine a
14 simple carbon monoxide (CO)-like tracer (COt) and its soluble version (SAt), both with the
15 2001 CO emissions, in simulations with the GFDL chemistry-climate model (AM3) for
16 present (1981-2000) and future (2081-2100) climates. In 2081-2100, projected reductions in
17 lower tropospheric ventilation and wet deposition contribute to exacerbating surface air
18 pollution as evidenced by higher surface COt and SAt concentrations. However, the average
19 horizontal general circulation patterns in 2081-2100 are similar to 1981-2000, so the spatial
20 distribution of COt changes little. Precipitation is an important factor controlling soluble
21 pollutant wet removal, but the total global precipitation change alone is not a sufficient
22 indicator of the soluble pollutant response to climate change. Over certain latitudinal bands,

23 however, the annual wet deposition change can be explained mainly by the simulated
24 changes in large-scale (LS) precipitation. In regions such as North America, differences in
25 the seasonality of LS precipitation and tracer burdens contribute to an apparent mismatch of
26 changes in annual wet deposition versus annual precipitation. We develop a diagnosed
27 precipitation impact (DPI) index to directly infer soluble pollutant wet deposition responses
28 from changes in precipitation as simulated by a climate model. Specifically, we express DPI
29 as the global mean of present-day pollutant burden weighted LS precipitation change divided
30 by the global mean of present-day pollutant weighted LS precipitation. This index captures
31 the sign and magnitude (within a factor of 2) of the relative annual and July mean changes in
32 the global wet deposition of the soluble pollutant. If our findings that LS precipitation
33 dominates wet deposition and that horizontal transport patterns change little in a future
34 climate are broadly applicable, the DPI could be applied to LS precipitation fields in other
35 climate models to obtain estimates of the distributions of soluble pollutants under future
36 scenarios. Our findings support the need for tighter emission regulations, for both soluble and
37 insoluble pollutants, to obtain a desired level of air quality as climate warms.

38 1. Introduction

39 Air quality is influenced by meteorological conditions and thus could be sensitive to
40 climate change [e.g., *Denman et al.*, 2007]. In the next few decades, models project
41 significant changes in global and regional climate [e.g., *Christensen et al.*, 2007; *Meehl et al.*,
42 2007], including increases in temperature, changes in the hydrological cycle, alterations in
43 global and regional circulation patterns (e.g., poleward expansion of the Hadley cell, reduced
44 tropical convective mass fluxes and reduced mid-latitude cyclone frequency). These changes
45 are expected to affect pollutant transport processes, natural pollutant precursor emissions that
46 depend strongly on meteorology (lightning NO_x, biogenic emissions), and the rates of
47 chemical reactions. Estimating the climate change impact on air quality requires a good
48 understanding of each of these processes.

49 Most General Circulation Model (GCM) and/or Chemical Transport Model (CTM)
50 studies of the impact of climate change on air pollutants focus on ozone (O₃) and particulate
51 matter (PM) because these two species are of most concern for human health and directly
52 affect both air quality and atmospheric radiative forcing [e.g., *Jacob and Winner*, 2009].
53 Under future climate, models agree that as a result of 21st-century climate change,
54 background O₃ in the lower troposphere (where O₃ loss by reacting with water vapor is
55 dominant) will decrease while surface O₃ over the polluted regions at northern mid-latitudes
56 will increase (+1-10 ppbv) [*Wu et al.*, 2008a, b; *Lin et al.*, 2008; *Nolte et al.*, 2008; *Weaver et*
57 *al.*, 2009]. For PM, models predict significant changes ($\pm 0.1-1 \mu\text{g m}^{-3}$) but neither the sign
58 nor the magnitude is consistent across models [*Jacob and Winner*, 2009]. The uncertainty
59 regarding the impact of climate on particulate matter reflects the complexity of the
60 dependence of its components on meteorological variables, and the key role of precipitation

61 in modulating PM sinks [*Racherla and Adams*, 2006; *Tagaris et al.*, 2007; *Avise et al.*, 2009;
62 *Pye et al.*, 2009; *Dawson et al.*, 2007]. Although *Racherla and Adams* [2006] showed that a
63 lower PM burden corresponds to an increase in global precipitation in a future climate, *Pye et*
64 *al.* [2009] indicated that changes in precipitation are not always the governing factor for PM
65 concentrations. *Jacob and Winner* [2009] argued that precipitation frequency is likely the
66 dominant factor determining PM concentration changes. Such disparate results in the
67 literature motivate our investigation into the impact of changing precipitation on soluble
68 pollutants in a warmer climate.

69 To isolate the roles of transport and precipitation, processes affecting many air
70 pollutants, idealized atmospheric tracers can be used to represent air pollutants in a climate
71 model. Previous studies have applied atmospheric tracers in GCMs to study the impact of
72 transport changes under climate change. For example, *Holzer and Boer* [2001] analyzed
73 tracers emitted from temporally constant localized surface sources. They find that inter-
74 hemispheric exchange times, mixing times, and mean transit times all increase under global
75 warming by about 10% from 1990–2000 to 2090–2100, but they consider only advection and
76 diffusion and neglect wet deposition and convection. Furthermore, their tracers have
77 localized (rather than distributed) sources, permitting the identification of transport pathways
78 from specific locations while precluding examination of the impact of spatial patterns in
79 precipitation and ventilation changes over polluted regions. *Rind et al.* [2001] examined
80 changes in the distributions of long-lived tracers (such as CO₂ and CFCs) in a doubled-CO₂
81 climate and found a 30% increase in troposphere-to-stratosphere transport and a decrease in
82 surface tracers due to enhanced convection. *Mickley et al.* [2004] incorporated black carbon
83 (BC) and CO-like tracers of fossil fuel emissions in a GCM and found that the severity and

84 duration of summertime regional pollution episodes in the Midwest and northeastern United
85 States increase significantly relative to the present due to decreased frequency of migratory
86 cyclones. So far, the impacts of projected precipitation changes on the burdens of soluble
87 pollutants, such as oxidized nitrogen, sulfate and nitrate aerosols, have not been isolated from
88 other climate impacts (e.g., chemical evolution, emission changes).

89 In this study, in order to investigate how pollutant distributions change due to
90 changing transport and precipitation in a warmer climate, we apply idealized tracers (with
91 insoluble and soluble versions) in a global chemistry-climate coupled model (Atmospheric
92 Model version 3, AM3, developed by the Geophysical Fluid Dynamics Laboratory (GFDL)),
93 a prototype of that described in *Donner et al.*, 2010. In section 2, we describe our model,
94 including the model parameterizations most relevant to this study and the experiments
95 conducted. Changes in the future distributions of soluble and insoluble tracers are described
96 and compared in section 3. Section 4 discusses the circulation changes that help redistribute
97 the insoluble tracer in a warmer climate. Section 5 shows our investigation on the impact of
98 precipitation changes on soluble tracer distributions. Conclusions are given in section 6.

99

100 **2. Methods**

101 **2.1 Model Description**

102 We use the GFDL AM3 model, a prototype of that described by *Donner et al.* [2010]
103 to examine the impact of climate change on tracer distributions. AM3 uses a finite-volume
104 dynamical core similar to that used in CM2.1 [*Delworth et al.*, 2006] but implemented on a
105 cubed-sphere grid [*Putman and Lin*, 2007]. The Earth is represented as a cube with six

106 rectangular faces and there is no singularity associated with the north and south poles as with
 107 the latitude-longitude representation, avoiding the need for polar filtering. The model
 108 horizontal resolution is C48 (48×48 cells per face); the size of the grid cell varies from ~163
 109 km (at the 6 corners of the cubed sphere) to 231 km (near the center of each face). The model
 110 used in our simulations has 48 vertical levels, with the top level centered at 1.7 Pa (~75km).

111 AM3 includes a different treatment of deep convection [*Donner et al.*, 2001; *Wilcox*
 112 *and Donner*, 2007] relative to AM2, the previous generation of the GFDL atmospheric model
 113 [e.g., *GAMDT* 2005]. Shallow convection is after *Bretherton et al.* [2004] with several
 114 modifications described in *Donner et al.* [2010]. The chemistry models of *Horowitz et al.*
 115 [2003] for the troposphere and *Austin and Wilson* [2006] for the stratosphere are merged into
 116 AM3. Wet deposition includes in-cloud and below-cloud scavenging by large-scale and
 117 convective clouds. The wet deposition flux (W) is directly proportional to the local
 118 concentration (C), given by $W = \Gamma \cdot C$, where Γ is the wet scavenging coefficient. In-cloud
 119 scavenging of aerosols is calculated following *Giorgi and Chameides* [1985]. The in-cloud
 120 scavenging coefficient is:

$$121 \quad \Gamma_{in} = 1 - \exp(-\beta \cdot f), \beta = \frac{P_{rain}^{k+1} - P_{rain}^k + P_{snow}^{k+1} - P_{snow}^k}{\Delta p \cdot g^{-1} \cdot x_{liq}} ;$$

122 where f is the scavenging factor, P^k is the precipitation flux through the top of layer k , P^{k+1}
 123 is the precipitation flux through the bottom of layer k (top of layer $k+1$) (thus, $P^{k+1} - P^k$ is the
 124 precipitation generated in layer k ; Δp is the pressure difference between model level k and
 125 $k+1$), g is the gravitational acceleration. The liquid water content x_{liq}
 126 ($= \frac{\text{precipitable water}(kg)}{\text{air}(kg)}$) is calculated by the large-scale cloud and convective

127 parameterizations. The fraction of aerosol incorporated in the raindrops and snow, f , is
128 prescribed. It ranges from 0.07 for dust to 0.2 for sulfate in large-scale clouds, and from 0.12
129 for dust to 0.5 for sulfate in convective clouds (note that these scavenging factors differ from
130 those used by *Donner et al.* [2010]). In case of convective precipitation, wet deposition is
131 only computed within the updraft plume. The f for trace gases is determined by Henry’s Law
132 equilibrium [*Donner et al.*, 2010]. Below-cloud washout is only considered for large-scale
133 precipitation and is parameterized as by *Li et al.* [2008] for aerosols with the below cloud
134 scavenging coefficient (Γ_{bc}) calculated as $\Gamma_{bc} = \frac{3}{4} \left(\frac{P_{rain} \cdot \alpha_{rain}}{R_{rain} \cdot \rho_{H_2O}} + \frac{P_{snow} \cdot \alpha_{snow}}{R_{snow} \cdot \rho_{snow}} \right)$, where P_{rain} and
135 P_{snow} are the precipitation fluxes, α is the efficiency with which aerosols are collected by
136 raindrops and snow with $\alpha_{rain} = 0.001$ and $\alpha_{snow} = 0.001$, R is the radius of cloud droplets
137 with $R_{rain} = 0.001$ m and $R_{snow} = 0.001$ m, ρ is density with $\rho_{H_2O} = 1000 \text{ kgm}^{-3}$ and
138 $\rho_{snow} = 500 \text{ kgm}^{-3}$. Below-cloud washout for trace gases is calculated based on Henry’s law
139 following *Brasseur et al.* [1998].

140

141 2.2 Experiments and Tracers

142 We conduct a pair of idealized simulations designed to magnify the climate change
143 signals relative to model internal variability. For the present-day climate (denoted as “1981-
144 2000”), we use a monthly 20-year mean annually invariant climatology of observed sea
145 surface temperature and sea ice from the Hadley Center to drive our AM3 simulation. For the
146 future climate (referred to as “2081-2100”), we add the 20-year mean monthly anomalies of

147 sea surface temperature and sea ice extent (calculated from a 19-model¹ IPCC AR4 A1B
148 scenario ensemble mean) to the present-day observed climatological values. Both simulations
149 are run for 21 years with the first year as spin-up. Emissions of aerosols and trace gases in
150 both simulations are kept at 1990 level except for the long-lived greenhouse gases (CO₂, N₂O
151 and CFCs), the concentrations of which follow the A1B scenario. CH₄ is set to the 1990
152 levels for tropospheric chemistry calculations, but to be the A1B 2090 level for radiation
153 calculation, thus distinguishing between the direct radiative impact of CH₄ forcing on the
154 circulation from its indirect chemical impacts (changing radiatively active tracers like O₃).
155 These settings allow us to study the effect of climate change on pollutants, distinguishing
156 such changes from anthropogenic emission changes. The AM3 simulated global surface
157 temperature increase from 1981-2000 to 2081-2100 by 2.7 K, consistent with the IPCC AR4
158 report (2.8 K and 6% increases of surface temperature and precipitation in the AR4 model
159 ensemble mean) [Meehl *et al.*, 2007].

160 To clearly diagnose the impact of circulation changes in 2081-2100 on pollutant
161 distributions, we use a passive COt tracer that decays exponentially with a 25-day lifetime.
162 The emissions of this COt tracer (Figure 1) mimic CO emissions in 2001, including
163 anthropogenic emissions from the RETRO project (Schultz *et al.*, 2007;
164 <http://www.retro.enes.org>) and biomass burning emissions from GFED version2 (van der
165 Werf *et al.*, 2006; <http://www.geo.vu.nl/~gwerf/GFED.htm>). Another tracer, SAt, follows the

¹ These models include CSIRO-Mk3.5 [Gordon *et al.*, 2002], INGV-ECHAM4 [Gualdi *et al.*, 2006] and the models in Table 1 (<http://ams.allenpress.com/perlserv/?request=get-abstract&doi=10.1175/JCLI4258.1>, except models number 10, 11, 12, 9 and 20).

166 same emission and decay as CO_t, but is subjected to additional removal by wet deposition as
167 for sulfate aerosols (Section 2.1). The application of these tracers is adapted from the
168 diagnostic tracer experiments (TP) of the Task Force on Hemispheric Transport of
169 Atmospheric Pollutants [*HTAP*, 2007; <http://www.htap.org>]. The total anthropogenic and
170 biomass burning CO emissions are about 1000 Tg CO yr⁻¹. In addition to the four regions
171 tagged as in the HTAP TP experiments (East Asia, South Asia, North America and Europe),
172 we tag three additional regions (central Africa, Southeast Asia and Russian Asia) to help us
173 identify the changes in transport pathway for different source regions (Figure 1).

174 The major advantages of our approach are: 1) the emissions of these tracers follow
175 the surface emissions of CO, including both anthropogenic and biomass burning emissions,
176 and their lifetimes are close to those of real pollutants, such as CO (CO_t) and sulfate aerosols
177 (SA_t); 2) the application of this pair of tracers, with and without wet deposition, helps us to
178 isolate the impact of precipitation in a future climate; 3) we use two 20-year simulations
179 driven by annually-invariant sea surface temperature and sea ice to maximize the detection of
180 a climate change signal relative to the internal model variability.

181

182 **3. The Redistribution of Insoluble and Soluble Pollutants in a Future Climate**

183 Figures 2a and 2b show the zonal mean distribution in 1981-2000 and its change from
184 1981-2000 to 2081-2100 for the CO_t and SA_t tracers respectively. During 1981-2000, both
185 CO_t and SA_t have maximum concentrations at the surface near the tropics and over the
186 northern hemispheric mid-latitudes, reflecting the emissions distribution (Figure 1). Wet
187 deposition is the major sink of SA_t, accounting for 70% of its total loss. Due to this

188 additional sink compared to COt, the SAt concentration drops much more rapidly away from
189 its sources. The mean tracer concentrations in the lower troposphere (below 500hPa) and in
190 the free troposphere (above 500hPa) are 19 and 13 ppbv, respectively, for COt vs. 7.4 and 0.3
191 ppbv for SAt in 1981-2000.

192 Any redistribution of COt in the 2081-2100 simulation reflects only circulation
193 changes in a future climate. At the surface, COt concentrations increase by up to 6 ppbv in
194 the tropics and up to 1.5 ppbv at northern hemispheric mid-latitudes (with the relative change
195 ranging from 2-7%). In the free troposphere, COt concentrations decrease with a maximum
196 reduction of up to 2 ppbv (-2 to -12% at 400hPa). Near the tropopause, a large increase in the
197 COt concentration (with a maximum of 2 ppbv) occurs. COt tracer generally decreases in
198 southern hemisphere. Although circulation changes redistribute COt, the global tropospheric
199 burden remains the same from 1981-2000 to 2081-2100 due to the fixed 25-day lifetime and
200 fixed emissions.

201 As will be shown in Section 5, the changes in tropospheric SAt distribution differ
202 strongly from that of COt because it undergoes wet deposition. SAt surface concentration
203 increases both in the tropics and at the northern hemispheric mid-latitudes, similar to COt,
204 but with a greater relative change (above 10%). The increased surface concentrations of SAt
205 and COt suggest that a warmer climate will contribute to degraded air quality in the future. In
206 the free troposphere and the southern hemisphere (where COt concentration decreases), the
207 SAt concentration increases. The tropospheric SAt burden increases from 17 to 19 Gg
208 (+12%) in the future, indicating a 12% increase of lifetime from the 1981-2000 to 2081-2100
209 (as emissions are identical). Since wet deposition by precipitation is the only difference
210 between these two tracers, the different changes between SAt and COt solely result from

211 future changes in precipitation. We will discuss next the causes of the redistribution of COt
212 (Section 4) and SAAt (Section 5) in the future climate simulation.

213

214 **4. The Impact of Changing Transport on Insoluble Pollutants (COt)**

215 To help understand the vertical redistribution of tropospheric COt (i.e., increases in
216 the lower troposphere and decreases in the free troposphere), we apply a two-box model
217 between the lower troposphere and the free troposphere. The boundary between these two
218 boxes is defined as 500 hPa level following *Held and Soden* [2006]. Mass conservation of
219 COt in the free troposphere box suggests a balance $\mu^F(c^L - c^F) = m^F c^F / \tau$, in which m^F is the
220 total air mass within the free troposphere box, τ is the 25-day lifetime, c^L and c^F are the mean
221 COt concentrations in the lower troposphere and the free troposphere respectively, and μ^F is
222 the mass flux exchange between the lower troposphere and the free troposphere. Assume that

223 the mass of the troposphere is fixed, the balance suggests $\frac{\delta\mu^F}{\mu^F} + \frac{\delta(c^F - c^L)}{c^F - c^L} \approx \frac{\delta c^F}{c^F}$. We use

224 the simulated tracer concentration in the model and calculate the values for the second term
225 on the left hand side, the COt concentration gradient change between free troposphere and
226 lower troposphere (+10%), and the first term on the right hand side, the relative change in the

227 free tropospheric COt concentration (-3%). We then calculate $\frac{\delta\mu^F}{\mu^F}$, i.e., the relative change

228 of the mass flux exchange between these two boxes to be -13%. According to model-
229 diagnosed tracer tendencies in the free troposphere, most (>90%) of the transport flux change
230 between the lower troposphere and the free troposphere comes from the advective tendency
231 rather than the convective tendency. This weaker contribution from convection is consistent

232 with the study of *Holzer and Boer* [2001], which shows a similar vertical redistribution of
233 their surface-emitted tracers by only considering advection and diffusion. Applying our
234 analysis to AM3-simulated water vapor as in *Held and Soden* [2006], we get a similar 14%
235 decrease in the lower troposphere-free troposphere mass flux exchange.

236 Regarding the decreasing tropospheric CO_t concentration in the southern hemisphere
237 in a future climate, we apply a similar two-box model, this time representing the troposphere
238 in the northern and southern hemispheres. A 2% decrease in the hemispheric flux exchange is
239 derived from this model. Inter-hemispheric transport and transport between the tropics and
240 extra-tropics are dominated by the Hadley circulation [*Bowman and Carrie*, 2002; *Bowman*
241 *and Erukhimova*, 2004; *Hess*, 2005]. Many previous studies indicate a weakened Hadley cell
242 [e.g., *Rind et al.*, 2001; *Holzer and Boer*, 2001; *Held and Soden*, 2006] under global
243 warming. Consistent with these results, the AM3-simulated Hadley cell (represented by the
244 20-year annual mean mass streamfunction, see Auxiliary Figure S1) weakens over the lower
245 troposphere (by less than 5%) [*Held and Soden*, 2006; *Vecchi and Soden*, 2007], resulting in
246 the reduced hemispheric flux exchange. The relative decrease in inter-hemispheric flux
247 exchange is much smaller than that of the vertical mass flux exchange between the lower
248 troposphere and the free troposphere (more than -10%), indicating that from a global or
249 hemispheric perspective, a warming climate affects vertical transport more than horizontal
250 transport.

251 The strongly increased CO_t near the northern hemispheric midlatitude tropopause is
252 found for most of the regional tracers we tag (Section2), suggesting that the processes
253 responsible for the enhanced CO_t concentration are common to most of the northern
254 hemispheric sources. Under global warming, the tropopause has been shown to move upward

255 [*Santer et al.*, 2003; *Lorenz and DeWeaver*, 2007]. From present-day to the future, the AM3-
256 simulated tropopause (identified as in *Reichler et al.* [2003], based on the World
257 Meteorological Organization (WMO) lapse-rate criterion) moves upward by 8 hPa in the
258 tropics and 20hPa over the northern high latitudes. We can plot the CO_t concentration
259 relative to the tropopause (as calculated separately in the present-day and future simulations)
260 by vertically interpolating the tracer concentration (Figure 3). The enhancement of CO_t
261 concentration near the tropopause is much smaller than that shown in Figure 2a, suggesting
262 that most of the increase in CO_t near the tropopause appearing in Figure 2a results from the
263 upward movement of the tropopause.

264

265 **5. The Impact of Changing Precipitation on Soluble Pollutants**

266 The distinctive differences in future changes of CO_t and SA_t discussed in Section 3
267 are caused by changes of precipitation (and the corresponding changes in wet deposition).
268 The increase of SA_t throughout the whole troposphere and the longer lifetime of SA_t are
269 consistent with the decrease of wet deposition (-5%) and the resulting increase (18%) in the
270 lifetime against wet deposition from present-day to the future. As the total global
271 precipitation increases in the future (+6%), the increasing SA_t burden and decreasing wet
272 deposition imply that, globally, precipitation is less effective at removing soluble tracers
273 (SA_t) in the future. In the following sections, the causes of this apparent disparity between
274 increased precipitation and decreased wet deposition are investigated. We first briefly
275 evaluate the AM3 model simulated precipitation and its change in 2081-2100 (section 5.1).
276 Next, we discuss the geographical distribution of the large-scale and convective precipitation

277 changes (section 5.2), the seasonality of the precipitation and SAt changes (section 5.3) and
278 the possible role of precipitation frequency (section 5.4). In section 5.5, we propose an index
279 to estimate changes in the global burden and wet deposition of soluble pollutants directly
280 from precipitation changes projected by climate models.

281

282 **5.1 Simulated Precipitation under Present and Future Climates**

283 *Donner et al.* [2010] have evaluated the AM3 simulated precipitation pattern and
284 show that despite a positive bias located over the tropics by 3-5 mm day⁻¹ and a global total
285 precipitation excess of 16%, AM3, in general, well captures the observed precipitation
286 pattern reported by the Version-2 Global Precipitation Climatology Project (GPCP v.2)
287 [*Adler et al.*, 2003]. The total global annual precipitation increases by 6% (about 2% K⁻¹)
288 from 1981-2000 to 2081-2100 in the AM3 simulations, consistent with *Meehl et al.* [2007]
289 (5%), *Held and Soden* [2006] and *Vecchi and Soden* [2007] (2% K⁻¹). Strong regionally
290 varying precipitation changes are predicted in previous studies: *Emori and Brown* [2005]
291 show that annual precipitation often increases by over 20% at high latitudes, as well as in
292 eastern Africa, central Asia and the equatorial Pacific in the IPCC AR4 model ensemble;
293 meanwhile, substantial decreases, reaching 20%, occur in the Mediterranean region [*Rowell*
294 *and Jones*, 2006], the Caribbean region [*Neelin et al.*, 2006] and the subtropical western
295 coasts of each continent. In general, our simulations (Figure 4a) are consistent with these
296 patterns, except in the Caribbean region, where AM3 predicts increased precipitation.
297 Disagreements between models as to whether the future climate will be wetter or drier exist
298 at the margins of climatologically wet and dry regions (e.g., in a 10° band extending from

299 latitudes centered at about 35°N in North America, 50°N in Europe, and 25°N in East Asia,
300 including highly polluted areas [*Held and Soden, 2006; Jacob and Winner, 2009;*
301 *Christensen et al., 2007*]. Therefore, the precipitation impact on soluble pollutants (such as
302 PM) over these places may be sensitive to the regional precipitation change predicted by
303 specific models [*Jacob and Winner, 2009*].

304 In addition to the spatial pattern of precipitation, the seasonal variation of the
305 precipitation change is also important for predicting future soluble tracer tendencies. *Meehl*
306 *et al.* [2007] show that the monthly precipitation over North America in most models
307 increases in January but decreases in July, consistent with our result (not shown). Their
308 study, nevertheless, shows that models are much less consistent in their estimates of seasonal
309 precipitation changes than in the annual mean.

310 *Donner et al.* [2010] pointed out that although the AM3 simulated precipitation
311 intensity distribution is generally consistent with that observed, it fails to capture high-
312 intensity events. Following the method of *Vecchi and Soden* [2007], we use daily output from
313 our model for all the land grid cells to calculate the distribution function using 20 bins, each
314 of which contains 5% of the total distribution, with the thresholds for each bin computed
315 using the present-day simulation. We use the same bin thresholds to compute change in the
316 frequency of occurrence of each bin in our future simulation (Figure 4b). Extreme
317 precipitation (precipitation above 85% quantile in the present-day simulation) occurs more
318 frequently in the future, while moderate precipitation (5-35% precipitation bins) occurs less
319 frequently, in agreement with the results shown by *Vecchi and Soden* [2007], *Meehl et al.*
320 [2007], *Pall et al.* [2007] and references therein. Changing precipitation frequency could
321 potentially be an important control on wet deposition [*Jacob and Winner, 2009*].

322 5.2 The Role of Large-scale vs. Convective Precipitation

323 We examine the impacts of changing precipitation on SAt wet deposition as a way to
324 understand the SAt burden change from present-day to the future. Figure 5 shows the
325 latitudinal distribution of the SAt burden, SAt wet deposition and precipitation over land.
326 The total precipitation is highest in the tropics, where it is dominated by convective
327 precipitation (red lines). Large-scale precipitation (blue lines) becomes a larger contribution
328 and is comparable to convective precipitation in the mid-latitudes. In contrast to the total
329 precipitation, SAt wet deposition has maxima both in the tropics and in the extra-tropics.

330 Wet deposition by large-scale precipitation clearly dominates the total wet deposition
331 of the soluble SAt tracer in our model. One possibility for the different impacts of large-scale
332 versus convective precipitation on wet deposition could be that convective precipitation tends
333 to occur over regions with lower tracer burden while large-scale precipitation dominates in
334 more highly polluted regions. However, Figure 6 shows that over some source regions, i.e.,
335 central Africa, South Asia, East Asia, Europe and North America, convective precipitation
336 either dominates or is comparable to that of large-scale precipitation.

337 The balance between large-scale and convective wet deposition also depends on the
338 parameterizations applied in the model. Our empirically chosen settings for sulfate
339 scavenging (Section 2.2) tend to make convective precipitation a more efficient scavenging
340 process than large-scale precipitation if they occur in the same area. However, convective
341 precipitation occurs only within sub-grid updraft plumes and only washes out pollutants
342 within those plumes (Section 2.2). In contrast, the higher cloud fraction in large-scale
343 precipitation allows for more widespread scavenging of pollutants. As a result, on a regional
344 scale, wet deposition by large-scale precipitation overwhelms that by convective

345 precipitation (Figure 5). Our conclusion differs from that of *Balkanski et al.* [1993], who
346 show a larger role for scavenging by convective precipitation (74%) as compared to large-
347 scale precipitation (12%) in contributing to the global ^{210}Pb sink in their model. The much
348 longer lifetime (3.5 years, therefore, a more uniform distribution over the globe of ^{210}Pb)
349 compared to our tracers (25 days) and the coarser resolution in their model ($4^\circ \times 5^\circ$) may
350 partly explain the difference in our findings. *Textor et al.* [2006] examined 9 models within
351 the AeroCom initiative (<http://dataipsl.ipsl.jussieu.fr/AEROCOM/>) and found that the
352 simulated large-scale wet deposition contributions to total wet deposition vary from 0.1 to
353 0.9. The lack of model agreement results from differences in many aspects of the models,
354 including the tracer emissions used, tracer lifetime, the simulation of precipitation types,
355 model resolutions and so on. The parameterization in wet removal process applied can be one
356 important factor contributing to the disagreement. Despite the large discrepancy in
357 convective wet deposition over total wet deposition ratio shown in *Textor et al.* [2006] study,
358 some recent studies tend to suggest a more important role from large-scale wet deposition: a
359 recent study by *Croft et al.* [2010, in preparation, Aerosol processing in convective and
360 stratiform clouds in ECHAM5-HAM] showed a similar ratio of large-scale wet deposition
361 (10%) to our study when they applied a more physically detailed representation of aerosol
362 wet scavenging by convective clouds into the ECHAM5-HAM model; *Leibensperger*
363 [personal communication, 2010] also found a minor role of convective precipitation to the
364 wet deposition of PM in GEOS-chem model, in which, the global annual mean large-scale
365 wet deposition accounts for 72% of the total sulfate aerosol depositions.

366 Noting that large-scale precipitation is more effective in washing out the SAtracer in
367 our model and that large-scale wet deposition largely represents the total wet deposition, we

368 compare the global annual large-scale precipitation change with the large-scale wet
369 deposition change from present-day to the future and find they are inconsistent (+6% large-
370 scale precipitation vs. -5% large-scale wet deposition). Therefore, global precipitation
371 changes (total, convective, or large-scale) are not good predictors for global changes in wet
372 deposition induced by a warming climate.

373 Total precipitation increases almost everywhere over land north of 20°S, due to
374 increased convective precipitation; large-scale precipitation decreases south of 20°N and
375 between 40 and 50°N while increasing elsewhere from present-day to the future (Figure 5,
376 middle row). The corresponding latitudinal wet deposition change follows that of large-scale
377 wet deposition change in most latitudinal bands with a correlation coefficient above 0.9 and a
378 root mean square difference of around 8%. This implies that the latitudinal variability of the
379 change in the large-scale precipitation can largely explain that of SAt wet deposition in a
380 future climate. Furthermore, in a recent observational study by *Lloyd* [2010], a general
381 declining tendency of sodium chloride wet deposition over the continental United States was
382 found and was attributed to some unknown factors related to climate change. While reduced
383 entrainment of sea salt into the atmosphere, or the changing transport of sea salt may
384 contribute to the lower sodium chloride wet deposition, another possible explanation may be
385 large-scale precipitation changes.

386 Despite the general consistency between zonal mean changes in large-scale
387 precipitation and the SAt wet deposition (Figure 5), opposite-signed changes occur in the
388 northern mid-latitudes (25-40°N), where annual wet deposition decreases while precipitation
389 increases. Since large-scale wet deposition accounts for more than 90% of total wet

390 deposition at northern mid-latitudes, from now on we will focus on large-scale wet
391 deposition.

392

393 **5.3 Seasonal Changes over North America**

394 The oppositely signed changes in annual wet deposition and large-scale precipitation
395 occur over mid-latitude regions, such as North America (Auxiliary S2). In order to examine
396 the cause of this apparent inconsistency over North America, we investigate the seasonality
397 of their changes (Figure 7). During January, the large-scale precipitation increases almost
398 everywhere over the inland eastern and central United States, and the wet deposition
399 increases consistently in general. Along the east coast, the large-scale precipitation and the
400 wet deposition both decrease. In July, large-scale precipitation and wet deposition both
401 decrease in the northern part of this region and over Mexico.

402 Figure 8 shows the seasonal cycle of SAt burden, precipitation and wet deposition
403 summed over all land boxes within North America. The annual mean large-scale
404 precipitation over this region increases under global warming, driven by the precipitation
405 increase during winter. However, during summer when the SAt burden is strongest, the
406 lower precipitation decreases wet deposition. Consequently, the annual wet deposition drops
407 (Figure 8). The seasonal variation of precipitation change combined with that of the SAt
408 burden leads to the apparent disagreement between annual mean changes in precipitation and
409 wet deposition.

410

411 **5.4 Changes in Precipitation Frequency over North America**

412 During winter, the agreement between the spatial patterns of changes in precipitation
 413 and wet deposition is weaker (Figures 7 and 8). *Dawson et al.* [2007] also found a weaker
 414 sensitivity in the concentration of PM in January than in July over the eastern United States
 415 when perturbing precipitation rates in their chemical transport model. *Jacob and Winner*
 416 [2009] argued that this sensitivity difference implies that precipitation frequency, rather than
 417 the precipitation intensity, is a dominant factor determining the wet scavenging of the soluble
 418 tracers. In this section, we evaluate the impact of precipitation frequency on wet deposition.
 419 The mean precipitation rate, $P_r = P_i \times P_f$, where P_i represents the intensity of precipitation in
 420 an average precipitation event and P_f represents the frequency of such precipitation events.
 421 Changes in precipitation rate in a future climate can be explained by changes in average
 422 precipitation intensity or in precipitation frequency: $\frac{\delta P_r}{P_r} = \frac{\delta P_i}{P_i} + \frac{\delta P_f}{P_f}$. The soluble tracer
 423 burden is much lower in January than in July (Figure 7 and 8). Meanwhile, the large-scale
 424 precipitation, which is more effective in washing out the soluble tracers, is much stronger
 425 than convective precipitation in January. It is likely that in January, wet deposition in some
 426 regions is already maximized with precipitation intensity during a single event (i.e.,
 427 increasing precipitation intensity cannot increase wet scavenging because all of the soluble
 428 pollutant has already been washed out). Wet deposition change is thus not sensitive to $\frac{\delta P_i}{P_i}$
 429 (and as a result, it is not consistent with $\frac{\delta P_r}{P_r}$). Instead, the precipitation frequency change
 430 ($\frac{\delta P_f}{P_f}$) plays a more important role. We count the number of January days with precipitation
 431 within 1981-2000 and 2081-2100 separately to represent daily precipitation frequency.

432 Figure 9a shows that the number of precipitation days during January over the United States
433 changes from present day to the future by a few percent (decreasing in the eastern Coastal
434 United States and the Great Lakes while increasing in the southern and western United
435 States). The relative change of precipitation frequency is generally much smaller than that of
436 precipitation intensity change (Figure 9b, calculated as $\frac{\delta P_i}{P_i} = \frac{\delta P_r}{P_r} - \frac{\delta P_f}{P_f}$). As mentioned in
437 section 5.3, in January, the wet deposition change is generally consistent with the
438 precipitation rate change, especially over the central United States (Figure 7). However, over
439 the Great Lakes, Maine, Southern Canada and New Brunswick, Canada, wet deposition
440 decreases while the precipitation rate increases (Figure 7). The decrease in wet deposition is
441 driven by a decrease of precipitation frequency (Figure 9a) and occurs despite an increase in
442 precipitation intensity (Figure 9b). Wet deposition is apparently not sensitive in the model to
443 the precipitation intensity over this area, therefore the increase in precipitation intensity does
444 not lead to increased wet deposition. However, over most regions such as south of 30°N
445 (Figure 7), changing precipitation intensity plays a major role. The spatial correlation
446 coefficient between the relative change of precipitation intensity and wet deposition in
447 January is 0.6 while between that of precipitation frequency and the wet deposition is only
448 0.2 over the United States.

449 Examining the percentage change in the number of precipitation days globally for 20
450 Januarys, we found reductions over most tropical and mid-latitude regions (Auxiliary Figure
451 S3). But the change is usually small (within 5%) except over the Middle East, Arabia and
452 West Africa (where the reduction can be above 30%) compared to that of wet deposition
453 (typically above 10%), suggesting precipitation frequency typically plays a minor role in
454 determining the change of wet deposition. Similar reduction occurs to the number of

455 precipitation days when we analyze the entire 20 year daily data rather than focusing on
456 January (not shown). The reduction of precipitation days and the increase of global
457 precipitation are consistent with the increases of precipitation intensity in a warming climate
458 [*Meehl et al.*, 2007].

459

460 **5.5 The Diagnosed Precipitation Impact Index**

461 We test here whether we can infer the changes in SAt wet deposition and burden in
462 the future directly from the present day tracer distribution and precipitation as well as the
463 precipitation change from the present to future. As mentioned in Section 2.1, the wet
464 deposition flux is directly proportional to the local concentration, and depends non-linearly
465 on the local precipitation production, particularly large-scale precipitation (as demonstrated
466 in Section 5.2). If we assume that the main climate change influence on soluble pollutants
467 occurs primarily through precipitation (the spatial distribution of the burden change due to
468 transport is small as demonstrated in Figure 2), then we can examine the possibility of using
469 the large-scale precipitation weighted by present-day SAt tracer burden to directly infer the
470 future SAt wet deposition change. Although the wet deposition change over each grid box is
471 affected by many processes other than local wet deposition (most notably, transport), the
472 spatial pattern of changes in the wet deposition is well correlated with that of the burden-
473 weighted large-scale precipitation change (the correlation coefficients for the global spatial
474 patterns are 0.6, 0.5 and 0.8 for annual, January and July, Figure 10). January has the
475 smallest correlation coefficient, which is consistent with the lower similarity shown in Figure
476 7. During January, both large-scale precipitation fraction (40%) and large-scale wet

477 deposition fraction (90%) are higher than in July (30% and 85%). If we separate the globe
478 into three regions (the tropics, the northern extra-tropics and the southern extra-tropics),
479 weaker correlations occur in each extratropical region during its wintertime, when the large-
480 scale precipitation is strong. This is consistent with our hypothesis in section 5.3 that wet
481 deposition during winters may not be as sensitive to the large-scale precipitation intensity or
482 rate change as in other seasons while it is more sensitive to precipitation frequency.

483 On the basis of the correlation shown above, we define a diagnosed precipitation
484 impact index (DPI) based on the present-day large-scale precipitation, its change in a future
485 climate and the present-day SAt burden: $DPI = \frac{\overline{B \cdot \Delta P_{ls}}}{B \cdot P_{ls}}$, where B represents the present-day
486 SAt burden, ΔP_{ls} and P_{ls} represents the change in large-scale precipitation and the present-
487 day large-scale precipitation and the overbar represents a spatial average. In January, DPI
488 does not work; it is opposite in sign of the relative change of wet deposition (+6% vs. -4%,
489 respectively), reflecting the relatively lower correlation coefficients shown above and a lower
490 sensitivity of wet deposition on large-scale precipitation during winter time (Section 5.4).
491 However, the DPIs are consistent in sign with the relative changes in global wet deposition
492 simulated annually and in July (annual and July DPIs are -6% and -11%, within a factor of 2
493 of the corresponding relative changes in wet deposition, -9% and -6%). The agreement
494 between the DPI and the wet deposition change annually and in July confirms that the large-
495 scale precipitation change determines the global wet deposition change from the 1981-2000
496 to 2081-2100 in our model. Thus this DPI index may be useful to predict the sign of future
497 changes in the global SAt wet deposition and burden directly from a present-day distribution
498 of SAt burden and large-scale precipitation as well as the simulated large-scale precipitation

499 change. The DPI index can be used only under 2 key assumptions that are valid in AM3
500 model: 1) large-scale precipitation dominated wet deposition and 2) precipitation frequency
501 is not important. With these assumptions, DPI works for July and annual cases (shown above)
502 and for April and October (not shown), however, it does not work for January.

503 We test the generality of this approach by applying it to another soluble pollutant
504 tracer (SA_{t12}), with the same sources as SA_t, but with a 12-day lifetime. The shorter lifetime
505 restricts its distribution close to the source regions. The DPI approach also works for SA_{t12}.
506 For example, annually, the DPI calculated for SA_{t12} is also negative (-10%) and it is
507 consistent with decreasing SA_{t12} wet deposition (-9%) in a future climate. Therefore, the
508 DPI approach for predicting the impact of precipitation change is also applicable to soluble
509 species with shorter lifetimes. Tracers with longer lifetimes require further study as transport
510 might play a greater role and limit the utility of the DPI approach.

511 This DPI index provides a simple way to examine the precipitation impact on soluble
512 pollutant distributions by using only precipitation fields from different climate models.
513 However, the relative importance of large-scale versus convective wet deposition is highly
514 inconsistent across models [e.g., *Textor et al.*, 2006]. Clearly, the DPI calculated using the
515 large-scale precipitation changes would not be relevant for a model in which convective
516 precipitation dominates wet deposition. Improved understanding and parameterizations of
517 wet deposition processes would allow for the development of a more broadly applicable DPI,
518 which further help to improve confidence in projecting impacts of precipitation changes on
519 wet deposition of soluble pollutants.

520

521 **6. Conclusions**

522 We have used the Atmospheric Model version 3 (AM3) [*Donner et al.*, 2010]
523 developed by the Geophysical Fluid Dynamics Laboratory (GFDL) to investigate how
524 changes in climate may drive pollutant distributions to change in a warmer climate. In order
525 to isolate climate-induced transport and precipitation changes and their implications for
526 atmospheric pollutant distributions, we incorporate a simple carbon monoxide (CO)-like
527 tracer (COt), with CO emissions and a fixed 25-day lifetime, and a soluble version of that
528 tracer (SAt) in the model for 1981-2000 and 2081-2100 meteorological conditions.

529 From a global and hemispheric perspective, a warming climate affects pollution
530 transport more in the vertical than in the horizontal (the inter-hemispheric exchange
531 decreases by only 2%) but the mass exchange between the lower troposphere and the free
532 troposphere decreases by 13%. Both surface COt and SAt concentrations increase (less than
533 5% and about 10%, respectively) near source regions, due to reduced boundary layer
534 ventilation and reduced wet deposition in a future climate. These results support prior
535 emphasis on the need for tighter emission regulations to achieve a desired level of air quality
536 as climate warms [e.g., *Holzer and Boer*, 2001; *Wu et al.*, 2008b]. A higher tropopause (8hPa
537 in the tropics and 20 hPa in the high latitudes) may lead to stronger forcing from radiatively
538 active pollutants.

539 In this model, large-scale precipitation dominates the wet scavenging of soluble
540 pollutants, even in the tropics where convective precipitation exceeds large-scale
541 precipitation. For this model, one therefore cannot use changes in total convective
542 precipitation as a predictive index for the sign of the changes in soluble tracer in a warmer

543 climate. Furthermore, we find that the global large-scale precipitation changes are not a good
544 indicator. Instead, the latitudinal wet deposition change largely follows the regional pattern
545 of large-scale precipitation (correlation coefficient for zonal annual mean large-scale
546 precipitation and tracer wet deposition change is above 0.9). We conclude that as climate
547 warms, the longer lifetime of soluble pollutants with respect to wet deposition is mostly due
548 to the simulated decrease in the large-scale precipitation over land.

549 The seasonality of precipitation changes also modulate its impact. For example, over
550 North America, precipitation and wet deposition both increase in January, and decrease in
551 July. The absolute magnitude of the precipitation change is greater in January, so annual
552 precipitation increases; the absolute magnitude of the wet deposition change is greater in
553 July, so annual mean wet deposition decreases. The agreement between the precipitation and
554 wet deposition changes over North America is weaker in January than in July, implying a
555 possible role for changing precipitation frequency in determining tracer wet removal in
556 winter, as shown to occur over the Great Lakes. However, precipitation frequency declines
557 only weakly (less than 10%) in most regions and seasons in the model, only weakly
558 contributing to the changes in wet deposition in most cases.

559 As wet deposition changes dominate the changes in soluble pollutant distribution
560 from 1981-2000 to 2081-2100 (as opposed to a transport-driven redistribution), we explore
561 the possibility of using SAt burden-weighted LS precipitation change to help evaluate the
562 precipitation impact on soluble tracer burden in a future climate. We find that SAt burden-
563 weighted LS precipitation change have a fairly good spatial correlation with SAt wet
564 deposition change in a future climate, particularly for the July and annual case ($r = 0.8$ and
565 0.6 respectively). We thus develop a diagnosed precipitation impact (DPI) index (the global

566 mean of present-day pollutant burden weighted LS precipitation changes (future-present)
567 divided by the global mean of present-day pollutant weighted LS precipitation) to directly
568 infer soluble pollutant wet deposition responses from changes in precipitation as simulated
569 by a climate model. This index captures the sign and magnitude (to a factor of 2) of the
570 relative changes in the global wet deposition of the soluble pollutant tracer. If our findings
571 that LS precipitation dominates wet deposition and that horizontal pattern transport pattern
572 changes little in a future climate are broadly applicable, the DPI could be applied to LS
573 precipitation fields in other climate models to obtain an estimate of the distribution of soluble
574 pollutants in future scenarios.

575 The robustness of any predictions of future soluble pollutant tendencies should be
576 evaluated with an ensemble of models. Climate models, however, are notoriously
577 inconsistent in their simulated seasonal and regional precipitation changes [*Christensen et*
578 *al.*, 2007]. Applying our diagnosed precipitation impact index to other models that have
579 precipitation change patterns available provides us a simple yet quantitative way to estimate
580 the impact of precipitation change in those models on soluble tracers in a future climate.
581 Such an approach, however, requires our finding that large-scale precipitation dominates wet
582 deposition to be broadly applicable. Given the discrepancy in large-scale versus convective
583 precipitation simulations across climate models and their relative importance in determining
584 wet deposition [*Textor et al.*, 2006], there is a critical need for observational studies to
585 advance our understanding of these processes and improve their representation in models.

586

586 **Acknowledgements**

587 The authors would like to thank the Task Force of Hemispheric Transport of Atmospheric
588 Pollutant, specifically Drs. Martin Schultz and Oliver Wild for putting together the HTAP
589 TP1x emissions and designing the tracer experiments. The authors also want to acknowledge
590 Drs. Leo Donner, Junfeng Liu and Yi Ming for helpful discussions.

591 **References:**

- 592 Adler, R.F., G.J. Huffman, A. Chang, et al. (2003), The version-2 global precipitation
593 climatology project (GPCP) monthly precipitation analysis (1979-present). *J.*
594 *Hydrometeorology*, 4, 1147-1167.
- 595 Austin, J., and R.J. Wilson (2006) Ensemble simulations of the decline and recovery of
596 stratospheric ozone, *J. Geophys. Res.*, 111, D16314, doi10.1029/2005JD006907
- 597 Avise, J., Chen, J., Lamb, B., et al. (2009), Attribution of projected changes in summertime
598 US ozone and PM_{2.5} concentrations to global changes, *Atmos. Chem. Phys.*, 9, 1111-
599 1124, doi:10.5194/acp-9-1111-2009
- 600 Balkanski, Y. J., D. J. Jacob, G. M. Gardner, et al. (1993), Transport and Residence Times of
601 Tropospheric Aerosols Inferred from a Global Three-Dimensional Simulation
602 of ²¹⁰Pb., *J. Geophys. Res.*, 98(D11), 20, 573–20, 586
- 603 Bowman, K. P., and G. D. Carrie (2002), The Mean-Meridional Transport Circulation of the
604 Troposphere in an Idealized GCM, *Journal of the Atmospheric Sciences*, 59(9), 13,
605 1502-1514, doi: 10.1175/1520-0469(2002)059<1502:TMMTCO>2.0.CO
- 606 Bowman, K. P., and T. Erukhimova (2004), Comparison of Global-Scale Lagrangian
607 Transport Properties of the NCEP Reanalysis and CCM3, *J. Clim.*, 17(5), 12, 1135-
608 1146, doi: 10.1175/1520-0442(2004)017<1135:COGLTP>2.0.CO
- 609 Brasseur, G.P., et al. (1998), MOZART, a global chemical transport model for ozone and
610 related chemical tracers: 1. Model description, *J. Geophys. Res.*, 103, 28,265-28,289
- 611 Bretherton, C.S., J.R.McCaa, and H. Grenier (2004), A new parameterization for shallow
612 cumulus convection and its application to marine subtropical cloud-topped boundary
613 layers. Part I: Description and 1D results. *Mon. Wea. Rev.*, 132, 864-882

614 Christensen, J.H., B. Hewitson, A. Busuioc, et al. (2007), Regional Climate Projections. In:
615 Climate Change 2007: The Physical Science Basis. Contribution of Working Group I
616 to the Fourth Assessment Report of the Intergovernmental Panel on Climate Change
617 [Solomon, S., D. Qin, M. Manning, Z. Chen, M. Marquis, K.B. Averyt, M. Tignor
618 and H.L. Miller (eds.)]. Cambridge University Press, Cambridge, United Kingdom
619 and New York, NY, USA.

620 Dawson, J.P., Adams, P.J., Pandis, S.N. (2007), Sensitivity of PM_{2.5} to climate in the
621 Eastern US: a modeling case study, *Atmos. Chem. Phys.* 7, 4,295–4,309

622 Delworth, Thomas L., et al. (2006), GFDL's CM2 Global Coupled Climate Models. Part I:
623 Formulation and Simulation Characteristics. *Journal of Climate*, 19, 643-674

624 Denman, K.L., G. Brasseur, A. Chidthaisong, et al. (2007), Couplings Between Changes in
625 the Climate System and Biogeochemistry. In: Climate Change 2007: The Physical
626 Science Basis. Contribution of Working Group I to the Fourth Assessment Report of
627 the Intergovernmental Panel on Climate Change [Solomon, S., D. Qin, M. Manning,
628 Z. Chen, M. Marquis, K.B. Averyt, M.Tignor and H.L. Miller (eds.)]. Cambridge
629 University Press, Cambridge, United Kingdom and New York, NY, USA

630 Donner, L. J., Bruce L. Wyman, Richard S. Hemler, et al. (2010), The Dynamical Core,
631 Physical Parameterizations, and Basic Simulation Characteristics of the Atmospheric
632 Component of the GFDL Global Coupled Model CM3, submitted to *J. Climate*, 2010.

633 Donner, L. J., C.J. Seman, and R.S. Hemler, 2001: A cumulus parameterization including
634 mass fluxes, convective vertical velocities, and mesoscale effects: Thermodynamic
635 and hydrological aspects in a general circulation model, *J. Climate*, 14, 3444-3463.

636 Emori, S., and S. J. Brown (2005), Dynamic and thermodynamic changes in mean and
637 extreme precipitation under changed climate, *Geophys. Res. Lett.*, 32, L17706,
638 doi:10.1029/2005GL023272.

639 Gualdi, S., et al. (2006). The main features of the 20th century climate as simulated
640 with the SGX coupled GCM. *Claris News* 4, 7–13 (2006).

641 Gordon, H. B. et al. (2002), The CSIRO Mk3 Climate System Model. Tech. Report 60
642 (CSIRO Atmospheric Research, Aspendale, Victoria, 2002)

643 Giorgi, F., and W. L. Chameides (1985), The Rainout Parameterization in a Photochemical
644 Model, *J. Geophys. Res.*, 90(D5), 7872–7880

645 Held, I. M., and A. Y. Hou (1980), Nonlinear axially symmetric circulations in a nearly
646 inviscid atmosphere, *J. Atmos. Res.*, 37, 515–533.

647 Held, I. M., and B. J. Soden (2006), Robust response of the hydrological cycle to global
648 warming, *J. Clim.*, 19, 5686– 5699

649 Hess, P. G. (2005), A comparison of two paradigms: The relative global roles of moist
650 convective versus nonconvective transport, *J. Geophys. Res.* 110(D20)

651 Holzer, M. and G. J. Boer (2001), Simulated changes in atmospheric transport climate. *J.*
652 *Climate*, 14:4398–4420

653 Horowitz, L.W., S. Walters, D. Mauzerall, et al. (2003), A global simulation of tropospheric
654 ozone and related tracers: description and evaluation of MOZART, version 2, *J.*
655 *Geophys. Res.*, 108, D24, doi.10.1029/2002JD002853

656 Jacob, D. J., and D. A. Winner (2009), Effect of climate change on air quality, *Atmospheric*
657 *Environment*, 43, 13.

658 Li, F., P. Ginoux, and V. Ramaswamy (2008) Distribution, transport, and deposition of
659 mineral dust in the Southern Ocean and Antarctica: Contribution of major sources. *J.*
660 *Geophys. Res.*, 113, doi:10.1029/2007JD009190.

661 Lin, J.-T., Patten, K.O., Hayhoe, K., et al. (2008), Effects of future climate and biogenic
662 emissions changes on surface ozone over the United States and China. *J. Appl.*
663 *Meteor. Climatol.*, 47, 1888–1909

664 Lloyd, P. J. (2010), Changes in the wet precipitation of sodium and chloride over the
665 continental United States, 1984–2006, *Atmospheric Environment*, 44, 3196-3206,
666 doi:10.1016/j.atmosenv.2010.05.016

667 Lorenz, D. J., and E. T. DeWeaver (2007), Tropopause height and zonal wind response to
668 global warming in the IPCC scenario integrations, *J. Geophys. Res.*, 112, D10119,
669 doi:10.1029/2006JD008087

670 Lu, J., G. A. Vecchi, and T. Reichler (2007), Expansion of the Hadley cell under global
671 warming, *Geophys. Res. Lett.* , 34, L06805, doi : 10. 1029/2006GL028443.

672 Meehl, G.A., T.F. Stocker, W.D. Collins, et al, 2007: Global Climate Projections. In: Climate
673 Change 2007: The Physical Science Basis. Contribution of Working Group I to the
674 Fourth Assessment Report of the Intergovernmental Panel on Climate Change
675 [Solomon, S., D. Qin, M. Manning, Z. Chen, M. Marquis, K.B. Averyt, M. Tignor
676 and H.L. Miller (eds.)]. Cambridge University Press, Cambridge, United Kingdom
677 and New York, NY, USA

678 Mickley, L. J., et al. (2004), Effects of future climate change on regional air pollution
679 episodes in the United States, *Geophys. Res. Lett.*, 31: L24103, doi:
680 10.1029/2004GL021216.

681 Neelin, J.D., et al., 2006: Tropical drying trends in global warming models and observations.
682 *Proc. Natl. Acad. Sci. U.S.A.*, **103**, 6110–6115

683 Nolte, C.G., Gilliland, A.B., Hogrefe, C., Mickley, L.J., 2008. Linking global to regional
684 models to assess future climate impacts on surface ozone levels in the United States.
685 *J. Geophys. Res.* 113, D14307

686 Pall P, et al., (2007), Testing the Clausius–Clapeyron constraint on changes in extreme
687 precipitation under CO₂ warming, *Clim Dynam*, 28:351–363, doi: 10.1007/s00382-
688 006-0180-2

689 Putman, W. M. and S.-J. Lin (2007): Finite-volume transport on various cubed-sphere grid. J.
690 *Comput. Phys.*, 227, 5578

691 Pye, H.O.T., Seinfeld, J.H., Liao, et al. (2009), Effects of changes in climate and emissions
692 on future sulfate-nitrate-ammonium aerosol levels in the United States. *J. Geophys.*
693 *Res.* 114, D01205, doi:10.1029/2008JD010701.

694 Racherla, P. N., and P. J. Adams (2006), Sensitivity of global tropospheric ozone and fine
695 particulate matter concentrations to climate change, *J. Geophys. Res.*, 111, D24103,
696 doi:10.1029/2005JD006939

697 Reichler, T., M. Dameris, and R. Sausen (2003), Determining the tropopause height from
698 gridded data, *Geophys. Res. Lett.*, 30(20), 2042, doi:10.1029/2003GL018240

699 Rind, D., J. Lerner, and C. McLinden (2001), Changes of tracer distributions in the doubled
700 CO₂ climate, *J. Geophys. Res.*, 106(D22), 28, 061–28, 079

701 Rowell, D.P., and R.G. Jones (2006), Causes and uncertainty of future summer drying over
702 Europe. *Clim. Dyn.*, 27, 281–299

703 Santer, B. D., et al. (2003), Behavior of tropopause height and atmospheric temperature in
704 models, reanalyses, and observations: Decadal changes, *J. Geophys.*
705 *Res.*, 108(D1), 4002, doi:10.1029/2002JD002258, 2003

706 Schultz, M. and Rast, S. (2007), Emission datasets and methodologies for estimating
707 emissions, available at: http://retro.enes.org/reports/D1-6_final.pdf

708 Tagaris, E., Manomaiphiboon, K., Liao, K.-J., et al. (2007), Impacts of global climate change
709 and emissions on regional ozone and fine particulate matter concentrations over the
710 United States. *J. Geophys. Res.* 112, D14312

711 Textor, C., M. Schulz, S. Guibert, et al. (2006), Analysis and quantification of the diversities
712 of aerosol life cycles within AeroCom. *Atmos. Chem. Phys.*, 6, 1777-1813,
713 doi:10.5194/acp-6-1777-2006

714 van der Werf, G. R., Randerson, J. T., Giglio, et al. (2006), Interannual variability in global
715 biomass burning emissions from 1997 to 2004, *Atmos. Chem. Phys.*, 6, 3423-3441,
716 doi:10.5194/acp-6-3423-2006, 2006

717 Vecchi, G. A. and B. J. Soden (2007), Global warming and the weakening of the tropical
718 circulation. *J. Climate*, 20:4316–4340.

719 Weaver, C. P. et al., 2009: A Preliminary Synthesis of Modeled Climate Change Impacts on
720 U.S. Regional Ozone Concentrations, *Bulletin of the American Meteorological*
721 *Society*, 90, 1843-1863

- 722 Wilcox, E.M., and L.J. Donner, 2007: The frequency of extreme rain events in satellite rain-
723 rate estimates and an atmospheric general circulation model. *J. Climate*, 20, 53-69
- 724 Wu, S., Mickley, L.J., Jacob, D.J., et al. (2008a), Effects of 2000–2050 changes in climate
725 and emissions on global tropospheric ozone and the policy-relevant background
726 ozone in the United States. *J. Geophys. Res.* 113, D18312
- 727 Wu, S., L. J. Mickley, E. M. Leibensperger, et al. (2008b), Effects of 2000–2050 global
728 change on ozone air quality in the United States, *J. Geophys. Res.*, 113, D06302,
729 doi:10.1029/2007JD008917

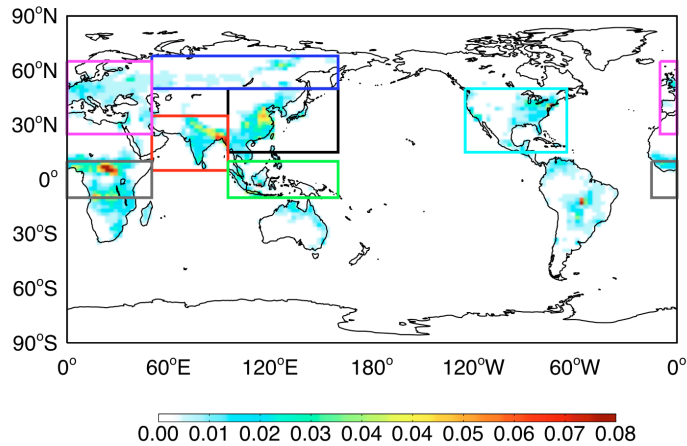


Figure 1. Annual mean COt emissions (unit: $10^{-1} \text{ mol/m}^2/\text{day}$, including both anthropogenic and biomass burning emissions [HTAP, 2007]. Tagged regions are shown as colored boxes.

730

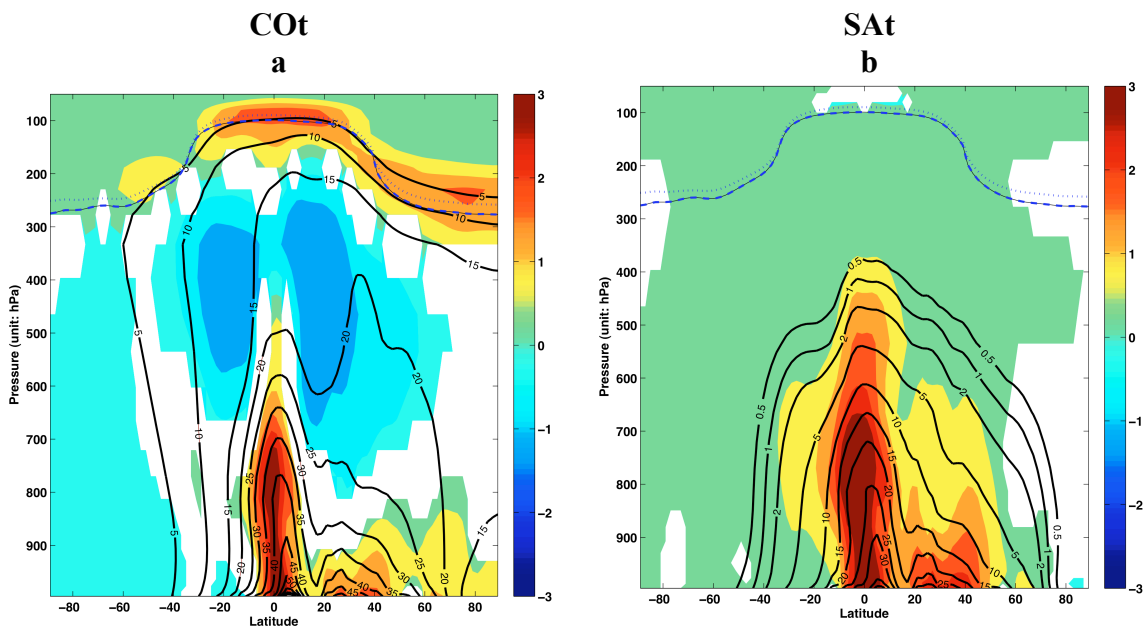


Figure 2. 20-year average zonal mean distribution of idealized tracer (unit: ppbv) during 1981-2000 (black solid contour) and the changes of that tracer from 1981-2000 to 2081-2100 (color shaded) with respect to vertical coordinates of pressure. (left, a) COt tracer, (right, b) SAt tracer. Blue dashed and dotted lines show the tropopause location during 1981-2000 and 2081-2100 respectively (identified as in Reichler *et al.* [2003], based on the World Meteorological Organization (WMO) lapse-rate criterion); only changes significant at the 95% confidence level assessed by t-test are shown).

731

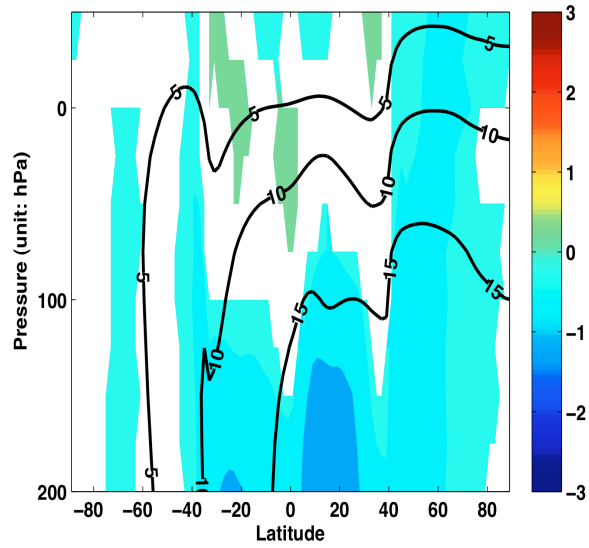


Figure 3. 20-year average zonal mean distribution of COt tracer (unit: ppbv) during 1981-2000 (black solid contour) and the changes of COt from 1981-2000 to 2081-2100 (color shaded) with respect to vertical coordinates of pressure difference from the tropopause; only changes significant at 95% confidence level assessed by t-test are shown).

732

733

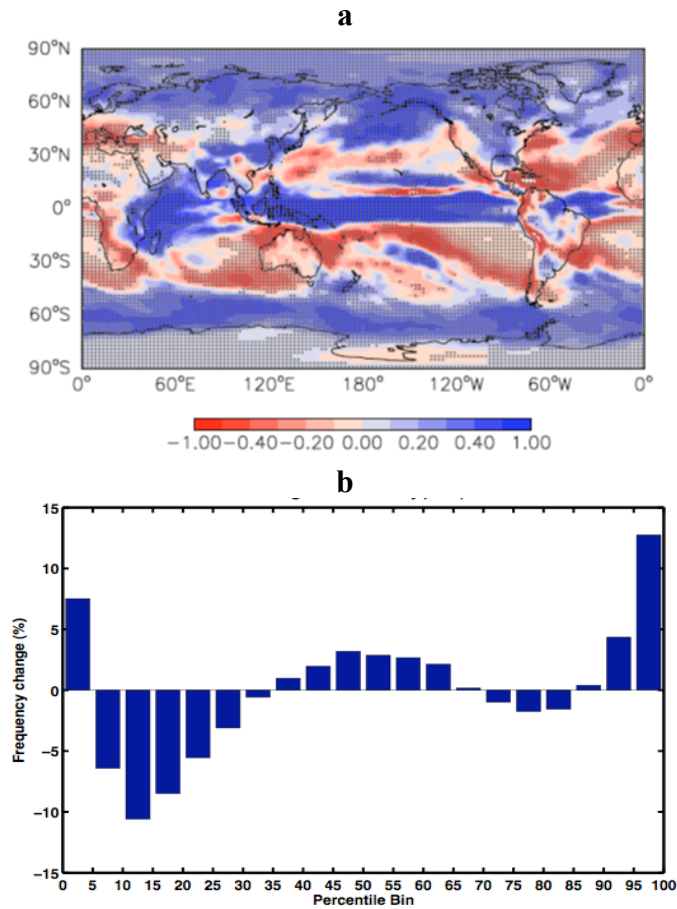


Figure 4. (a) The 20-year annual mean precipitation change from 1981-2000 to 2081-2100 (unit: mm/day, shaded area indicates the changes significant at the 95% confidence level assessed by t-test) and (b) the percentage change in the frequency of occurrence of precipitation as a function of precipitation intensity, using daily output over all land grid cells. The distribution function was calculated using 20 bins, each of which contains 5% of the total distribution for the present simulation (e.g., 0%–5%, 5%–10%, etc.). The thresholds for each bin were computed for 1981-2000 and then these thresholds were applied to compute the distribution over 2081–2100.

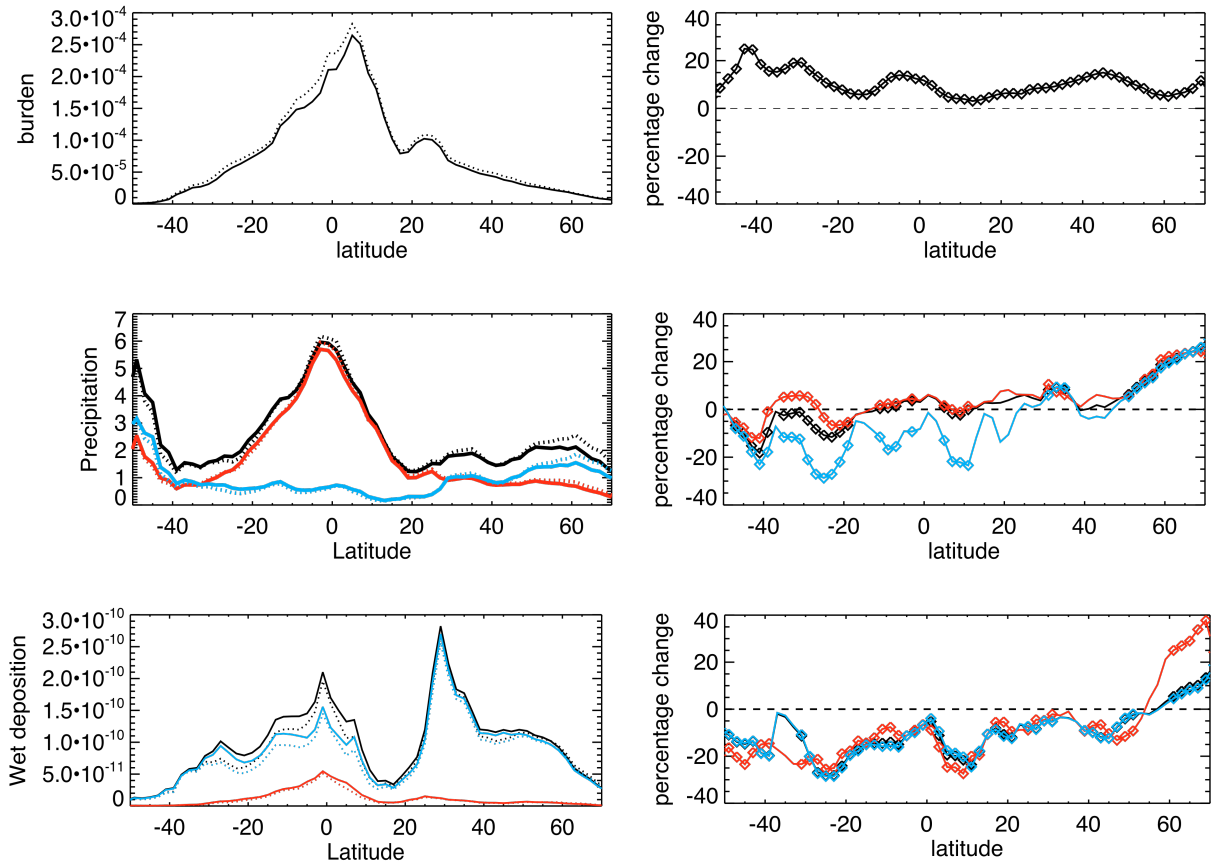


Figure 5. (Left panel) The 20-year annual mean latitudinal distribution of SAt burden (kg/m^2 , top) precipitation (mm/day , middle) and wet deposition ($\text{kg}/\text{m}^2/\text{day}$, bottom) over land: total, large-scale and convective precipitation/wet deposition shown in black, blue and red respectively; solid lines and dashed lines represent 1981-2000 and 2081-2100 cases respectively. (Right panel) The percentage change by 2081-2100 of the 20-year mean SAt burden (top), precipitation (middle) and SAt wet deposition (bottom), diamonds on each line represent the signals significant at the 95% confidence level, assuming that these annual data are independent.

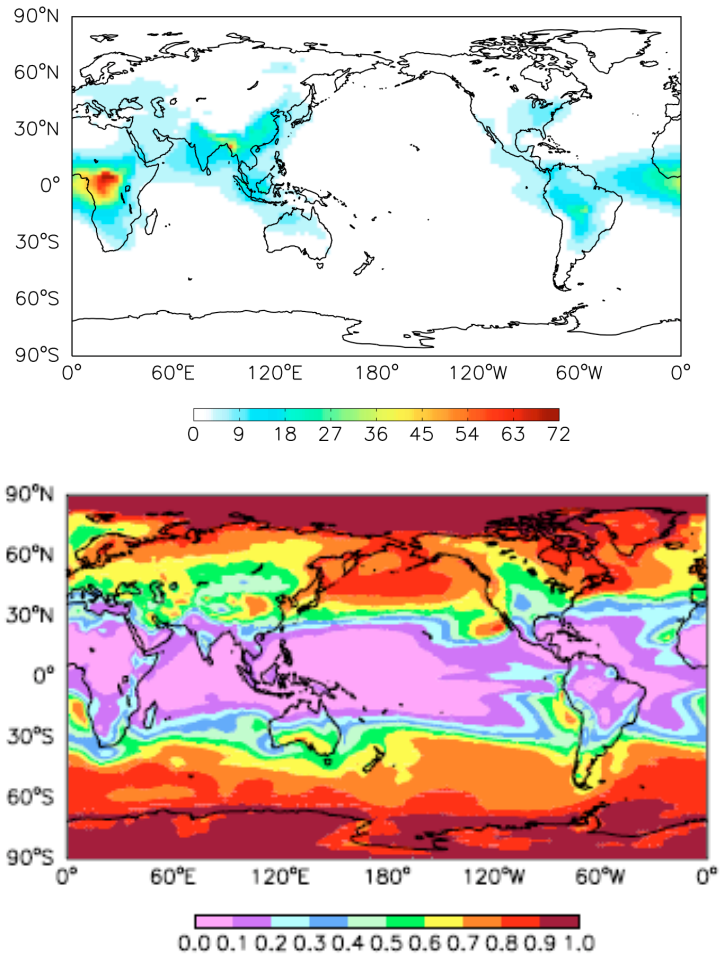


Figure 6. The 20-year annual mean distribution of SAt burden (unit: $10^{-5} \text{ kg m}^{-2}$) during 1981-2000 (top) and the 20-year mean fraction of precipitation that is large-scale (bottom)

735

736

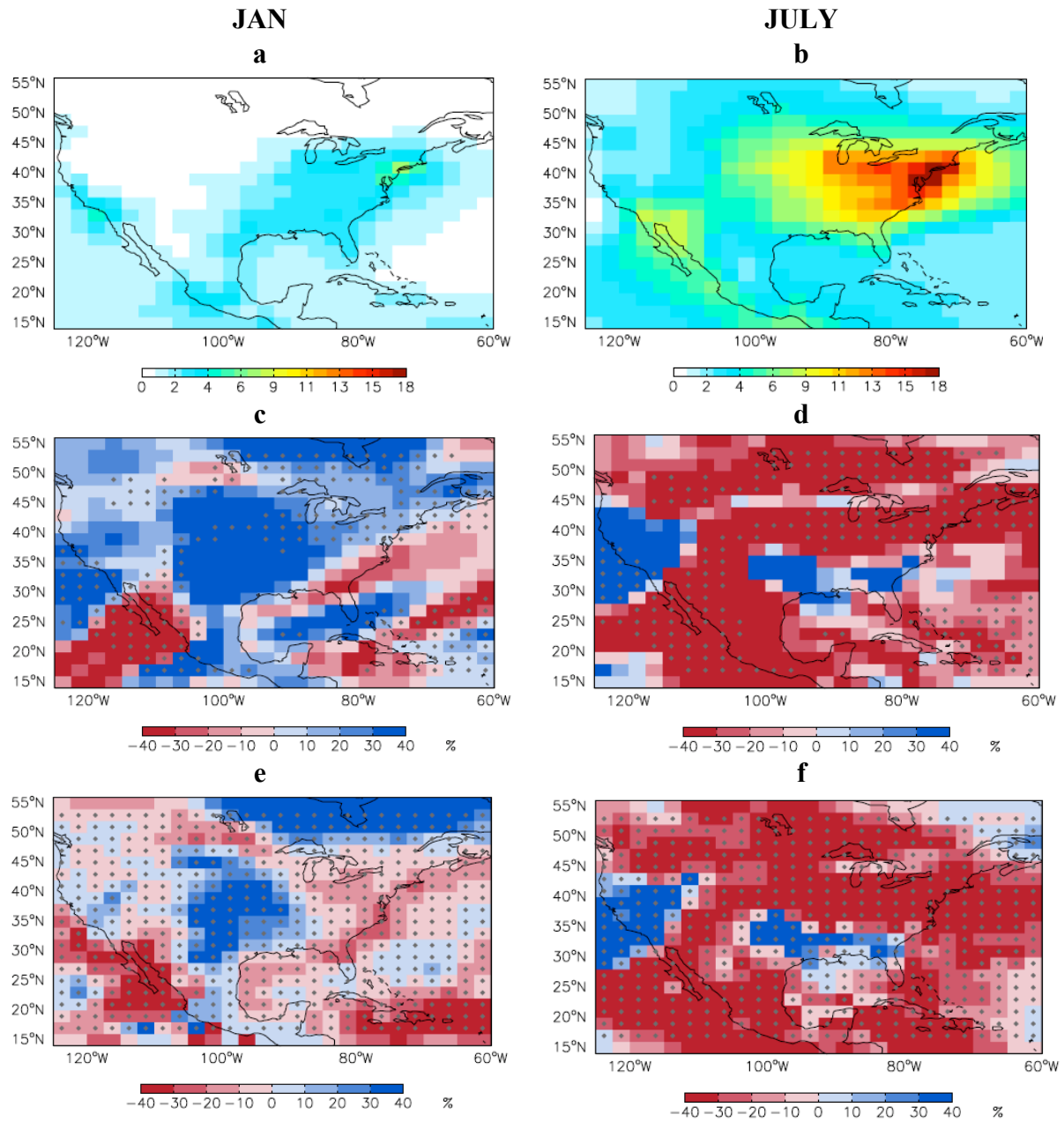


Figure 7. 20-year mean January (left) and July (right) SAt burden in 1990s (top, unit: 10^{-5} kg/m^2), large-scale precipitation percentage change (middle) and large-scale wet deposition percentage change (bottom), dotted area indicates changes significant at the 95% confidence level assessed by t-test. The maximum reduction of large-scale precipitation and wet deposition in July is about 100% and 90% while in January both are about 70%.

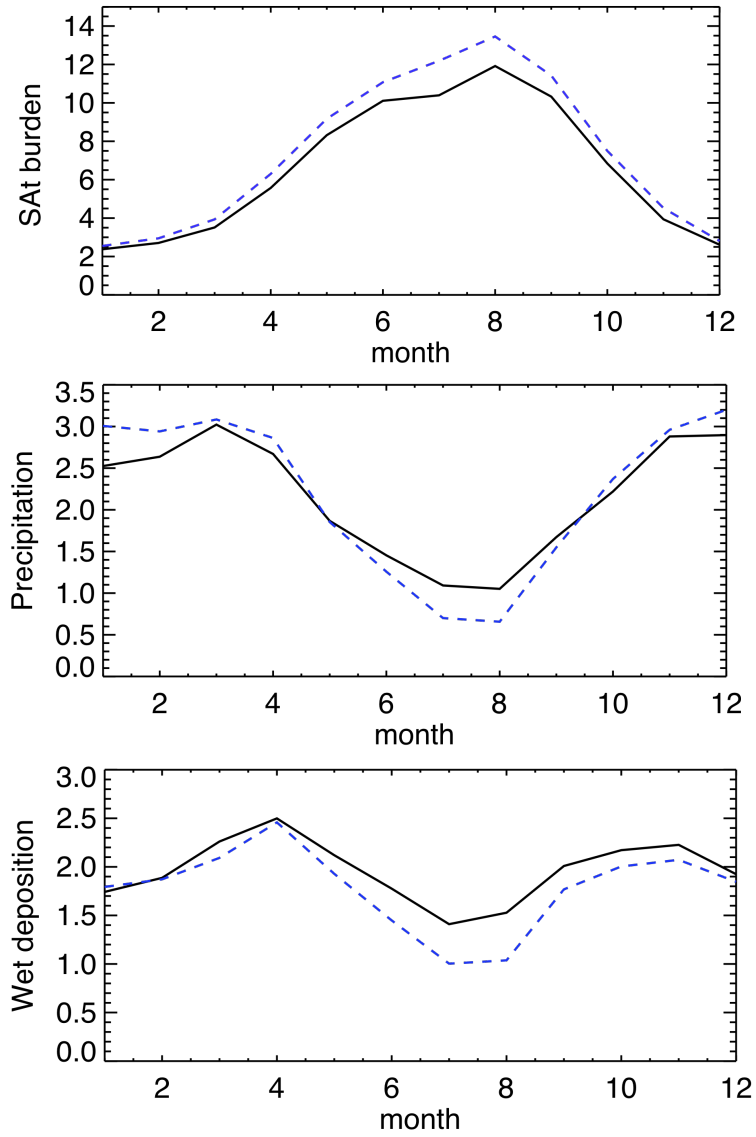


Figure 8. The 20-year mean seasonal cycle of total SAt burden (top, unit: 10^{-5}kg/m^2), precipitation (middle, unit: mm/day) and wet deposition (bottom, unit: $10^{-10} \text{kg/m}^2/\text{day}$) over land within North America during 1981-2000 (black solid) and 2081-2100 (blue dashed).

739

740

740

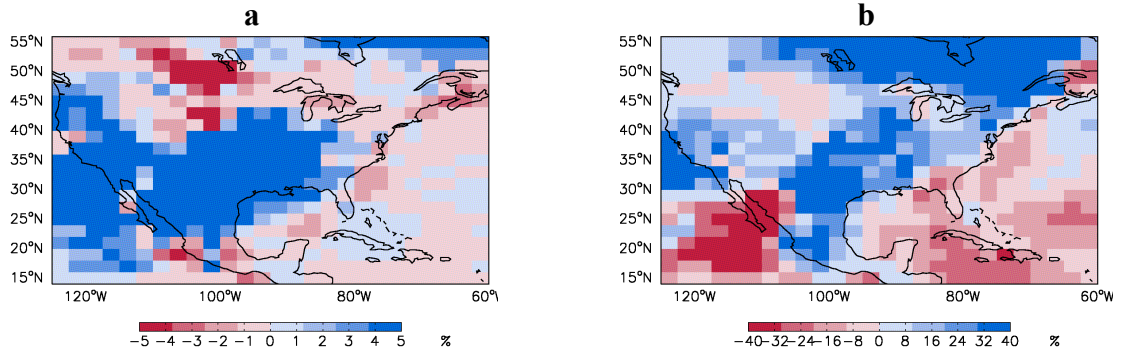


Figure 9. Percentage change of (a) the number of days with large-scale precipitation in all Januarys and (b) the large-scale precipitation intensity (calculated as the difference between the relative changes in large-scale precipitation (Figure 7c) and precipitation frequency (Figure 9a)) in January from 1981-2000 to 2081-2100 (unit: %); note different color scales

741

742

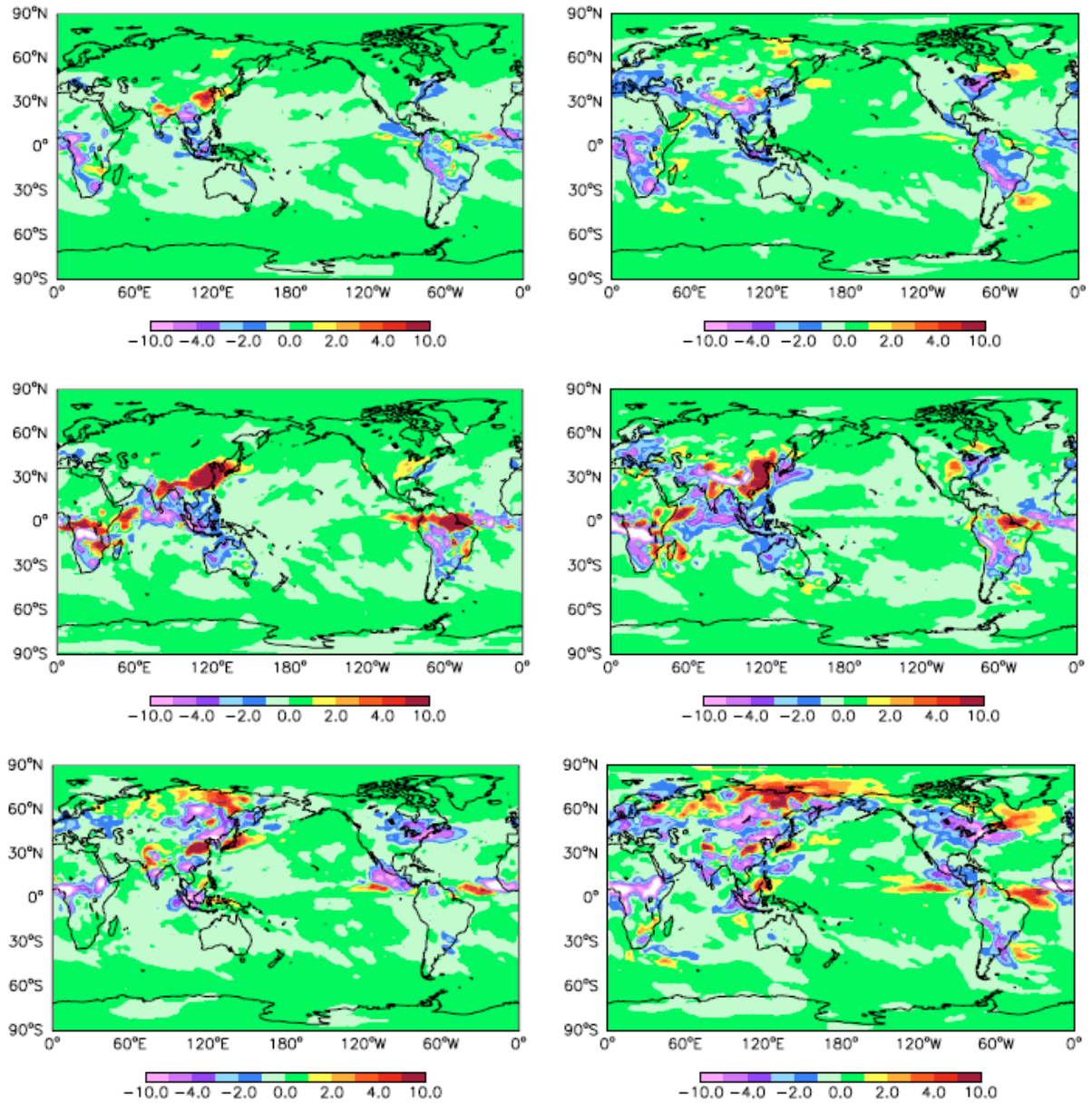


Figure 10. 20-year annual mean (top), January mean (middle) and July mean (bottom) diagnosed precipitation impacts (left, unit: $10^{-5} \text{ kg/m}^2 \cdot \text{kg/m}^2/\text{day}$) and wet deposition change (right, unit: $10^{-6} \text{ kg/m}^2/\text{day}$)

743

Auxiliary Material

744

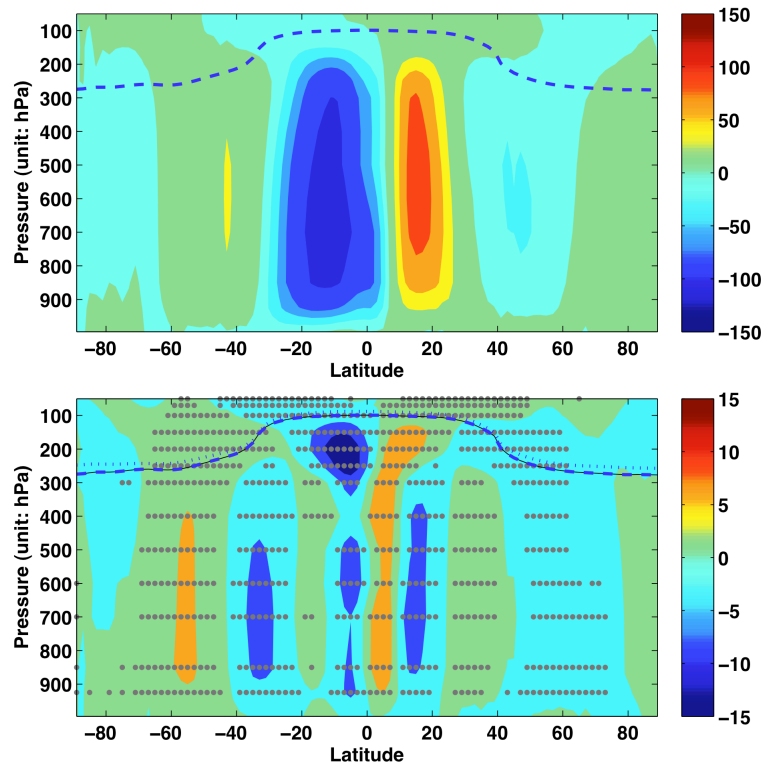


Figure S1. (top) 20-year average zonal mean distribution of mass streamfunction (unit: 10^9 kg/s) during 1981-2000 and (bottom) its change from 1981-2000 to 2081-2100 (dotted area indicates the changes significant at the 95% confidence level assessed by t-test)

745

746

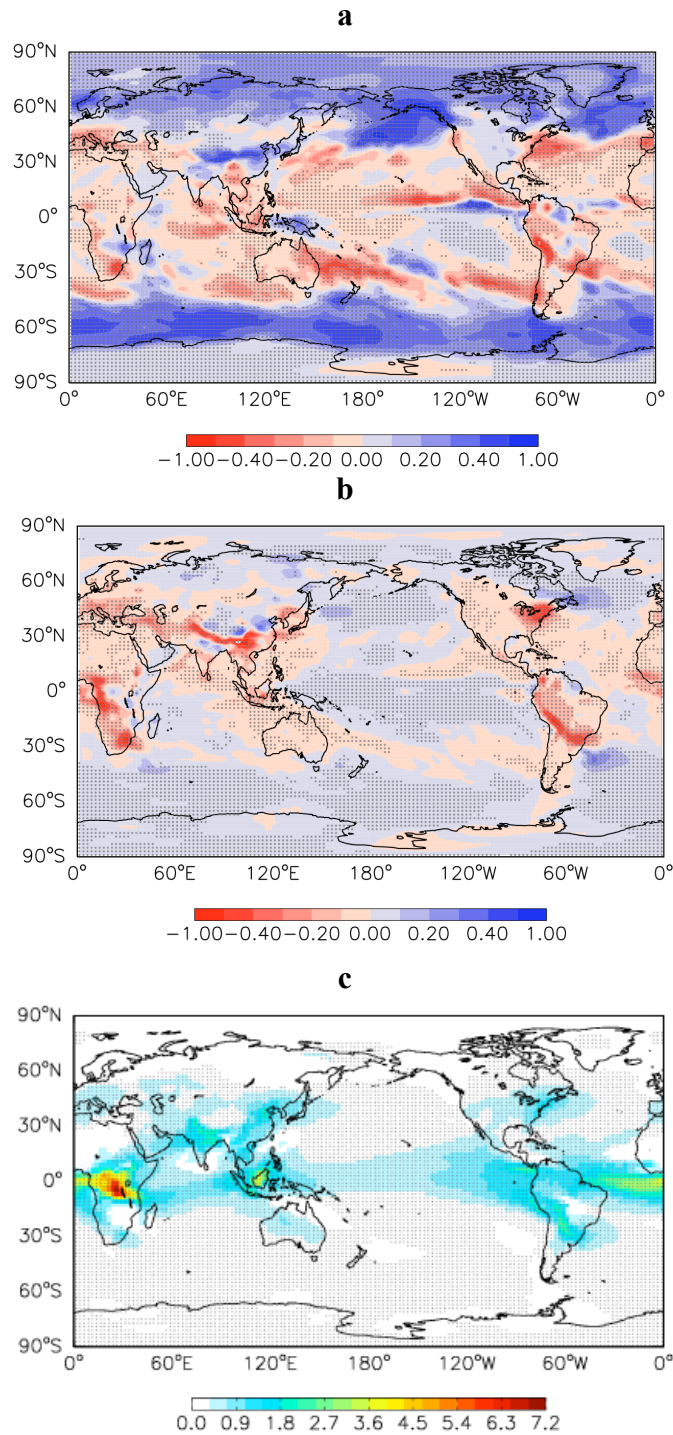


Figure S2. The 20-year annual mean changes (from 1981-2000 to 2081-2100) of (a) large-scale precipitation (unit: mm/day), (b) large-scale SAt wet deposition (unit: 10^{-5} kg/m²/day) and (c) SAt burden (10^{-5} kg/m²), dotted area indicates changes satisfying the 95% confidence level assessed by t-test.

747

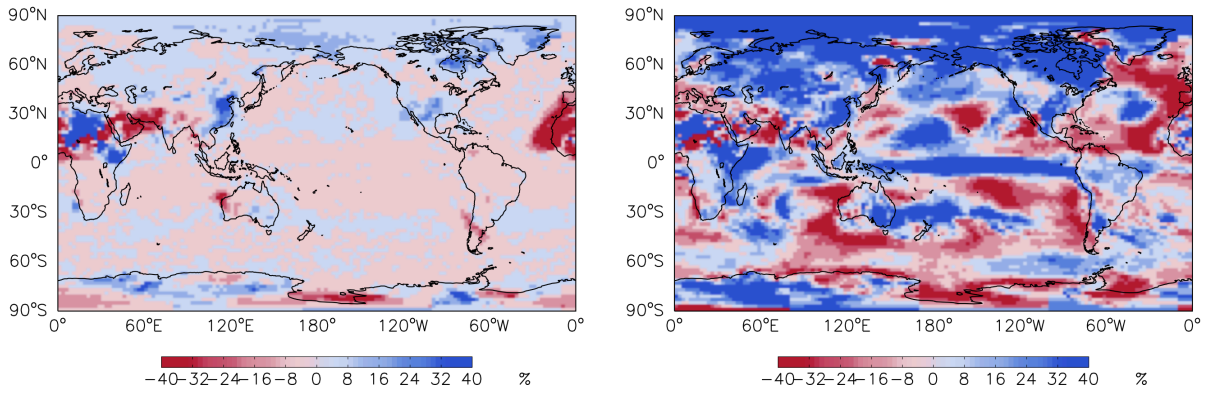


Figure S3. The percentage change of LS precipitation days (left) and the percentage change of LS precipitation intensity (right) during Januarys (Future – Present).

748